Helmholtz-Zentrum
Geesthacht
Zentrum für Material- und Küstenforschung

Original

Shibley, N.C.; Timmermans, M.-L.; Carpenter, J.R.; Toole, J.M.:

Spatial variability of the Arctic Ocean's double-diffusive staircase

Journal of Geophysical Research : Oceans (2017) AGU

DOI: 10.1002/2016JC012419

AGU PUBLICATIONS

JGR

Journal of Geophysical Research: Oceans

RESEARCH ARTICLE

10.1002/2016JC012419

Key Points:

- The double-diffusive staircase is characterized across the Arctic Ocean through an analysis of Ice-Tethered Profiler data from 2004 to 2013
- Bulk staircase properties are set by the large-scale Arctic Ocean circulation
- We examine where double-diffusive flux laws may be valid and hypothesize about what factors influence staircase features

Correspondence to:
N. C. Shibley,
nicole.shibley@yale.edu

Citation:
Shibley, N. C., M.-L. Timmermans, J. R. Carpenter, and J. M. Toole (2017), Spatial variability of the Arctic Ocean's double-diffusive staircase, *J. Geophys. Res. Oceans*, *122*, 980–994, doi:10.1002/2016JC012419.

Received 4 OCT 2016
Accepted 17 JAN 2017
Accepted article online 25 JAN 2017
Published online 8 FEB 2017

© 2017. American Geophysical Union. All Rights Reserved.

Spatial variability of the Arctic Ocean's double-diffusive staircase

N. C. Shibley[1], M.-L. Timmermans[1], J. R. Carpenter[2], and J. M. Toole[3]

[1]Department of Geology and Geophysics, Yale University, New Haven, Connecticut, USA, [2]Institute of Coastal Research, Helmholtz-Zentrum Geesthacht, Geesthacht, Germany, [3]Department of Physical Oceanography, Woods Hole Oceanographic Institution, Woods Hole, Massachusetts, USA

Abstract The Arctic Ocean thermohaline stratification frequently exhibits a staircase structure overlying the Atlantic Water Layer that can be attributed to the diffusive form of double-diffusive convection. The staircase consists of multiple layers of O(1) m in thickness separated by sharp interfaces, across which temperature and salinity change abruptly. Through a detailed analysis of Ice-Tethered Profiler measurements from 2004 to 2013, the double-diffusive staircase structure is characterized across the entire Arctic Ocean. We demonstrate how the large-scale Arctic Ocean circulation influences the small-scale staircase properties. These staircase properties (layer thicknesses and temperature and salinity jumps across interfaces) are examined in relation to a bulk vertical density ratio spanning the staircase stratification. We show that the Lomonosov Ridge serves as an approximate boundary between regions of low density ratio (approximately 3–4) on the Eurasian side and higher density ratio (approximately 6–7) on the Canadian side. We find that the Eurasian Basin staircase is characterized by fewer, thinner layers than that in the Canadian Basin, although the margins of all basins are characterized by relatively thin layers and the absence of a well-defined staircase. A double-diffusive 4/3 flux law parametrization is used to estimate vertical heat fluxes in the Canadian Basin to be O(0.1) W m^{-2}. It is shown that the 4/3 flux law may not be an appropriate representation of heat fluxes through the Eurasian Basin staircase. Here molecular heat fluxes are estimated to be between O(0.01) and O(0.1) W m^{-2}. However, many uncertainties remain about the exact nature of these fluxes.

1. Introduction

Arctic climate processes are strongly influenced by the existence and persistence of Arctic sea ice [*Perovich et al.*, 2013], which is influenced by ocean heat content and transports. Water entering the Arctic from the Atlantic Ocean is a significant source of this heat [e.g., *Rudels et al.*, 2004]. The distribution and fluxes of Atlantic Water Layer heat are central elements of the Arctic Ocean heat budget. This study examines the temperature and salinity structure at the upper boundary of the Atlantic Water Layer (the Arctic Ocean's thermocline), from which inferences about vertical ocean heat fluxes, and their spatial distribution, can be made.

The heat transfer from the Atlantic Water Layer to the upper ocean (and then to the sea ice) could have a substantial effect on sea ice thickness [e.g., *Aagaard et al.*, 1981; *Rudels et al.*, 2004; *Carmack et al.*, 2015]. In fact, there is sufficient heat contained in the Atlantic Water Layer that if it could be fluxed to the surface ocean in contact with sea ice, it would melt the entire sea-ice pack [*Maykut and Untersteiner*, 1971]. However, at present, a strong density stratification (primarily due to salinity—the Arctic halocline) effectively insulates the surface ocean from Atlantic Water Layer heat in the central basins of the Arctic [e.g., *Aagaard et al.*, 1981; *Padman and Dillon*, 1987; *Timmermans et al.*, 2008; *Fer*, 2009]. In the center of the Arctic's Canada Basin, vertical heat fluxes from the Atlantic Water Layer are negligible compared to typical summer ocean-to-ice heat fluxes at the surface [e.g., *Timmermans et al.*, 2008]. In the Eurasian Basin on the other hand, Atlantic Water Layer heat fluxes are believed to be an important factor in contributing to sea ice decline [*Lenn et al.*, 2009; *Polyakov et al.*, 2012].

The average Atlantic Water Layer maximum potential temperature θ_{max} in the Amundsen Basin is around 1.3°C (where the depth of the θ_{max} is approximately 280 m), and in the Canadian Basin the average θ_{max} is around 0.7°C (where the depth of the θ_{max} is approximately 390 m; Figure 1). Atlantic Waters have a general

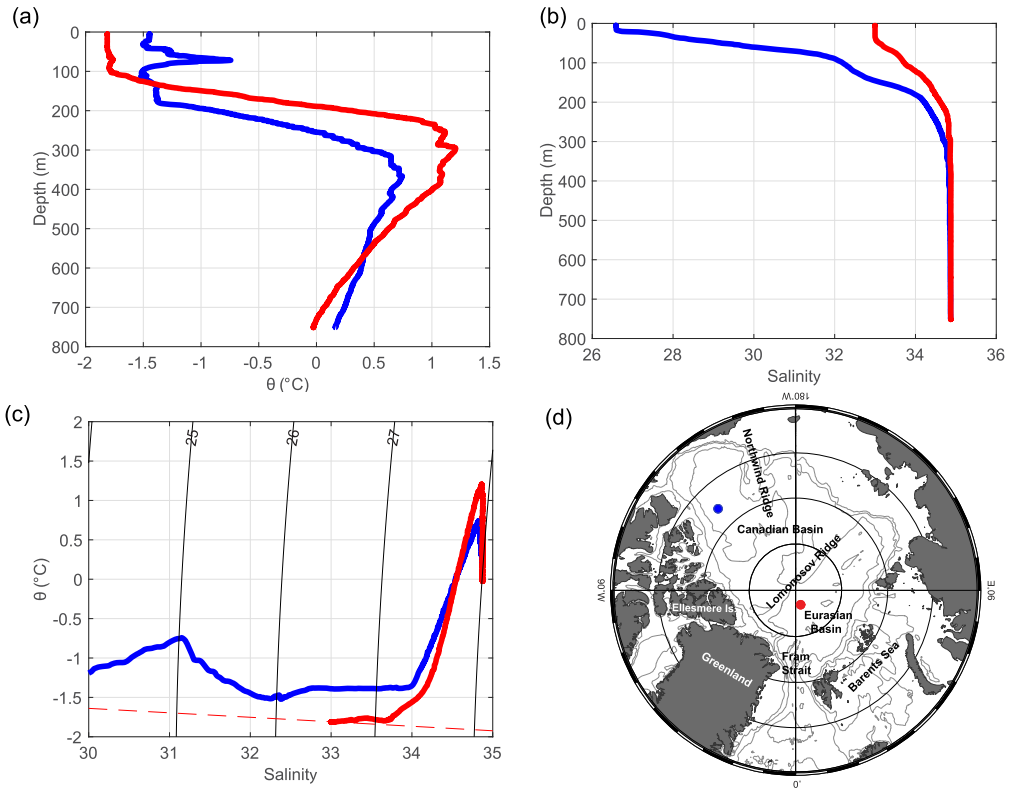

Figure 1. (a) Potential temperature θ (°C) and (b) salinity profiles in the central Eurasian Basin (red), where the θ_{max} of the Atlantic Water Layer is around 300 m depth, and central Canadian Basin (blue), where the θ_{max} of the Atlantic Water Layer is around 400 m. (c) The same representative profiles in θ-S space from the Eurasian Basin (red) and Canadian Basin (blue). Isopycnals (potential density anomaly in kg m^{-3}) are labeled, and the dashed red line is the freezing line. Profiles are from Ice-Tethered Profiler measurements in spring 2008. (d) Geographic features of the Arctic Ocean. The blue dot corresponds to the Canadian Basin profile shown, and the red dot corresponds to the Eurasian Basin profile shown.

inferred cyclonic circulation around the Arctic Basin from where they enter through Fram Strait and the Barents Sea opening. Where the Lomonosov Ridge reaches the edge of the Russian continental shelf, the Atlantic inflow splits into two cyclonic flows: one with waters circulating the entire Canadian Basin, and the other with waters circulating the Eurasian Basin along the Lomonosov Ridge, and back toward Fram Strait [e.g., *Rudels et al.*, 1994; *McLaughlin et al.*, 2004].

Above the depth of the Atlantic Water Layer θ_{max}, both temperature and salinity increase with depth and the water column is prone to the diffusive form of double-diffusive convection [e.g., *Turner and Stommel*, 1964; *Schmitt*, 1994; *Radko*, 2013]; throughout much of the central Arctic Basin, there exists a double-diffusive staircase at the top boundary of the Atlantic Water Layer, which has been well studied [e.g., *Melling et al.*, 1984; *Padman and Dillon*, 1987, 1988; *Timmermans et al.*, 2008; *Polyakov et al.*, 2012]. The double-diffusive staircase can be characterized by a density ratio, which is a measure of the change in density due to salinity across the staircase to the change in density due to temperature [e.g., *Turner*, 1965]. If the stabilizing effect of salinity is larger than the destabilizing effect of temperature (i.e., the density ratio is larger than 1 and the ocean is statically stable), double-diffusive staircases may be found in the ocean for density ratios up to ≈10 [e.g., *Kelley et al.*, 2003].

The Atlantic Water Layer staircase is characterized by well-mixed homogeneous layers generally between about 0.5 and 3.5 m thick, separated by high gradient interfaces across which potential temperature and salinity change by $\delta\theta \approx 0.04$°C and $\delta S \approx 0.01$, respectively. The double-diffusive heat flux through the staircase may be estimated by computing the fluxes through individual interfaces, employing a parametrization (a 4/3 flux law which is proportional to $\delta\theta^{4/3}$) that depends on the potential temperature and salinity jumps across the interfaces [*Kelley*, 1990]. Reported Atlantic Water Layer double-diffusive heat flux estimates range from 0.02 to 0.3 W m^{-2} in the Canada Basin [*Padman and Dillon*, 1987; *Timmermans et al.*, 2008], to

approximately 8 W m^{-2} north of the Laptev Sea [*Polyakov et al*., 2012] and O(0.1) W m^{-2} in the Amundsen Basin [*Guthrie et al*., 2015]. These estimates are based on both direct microstructure measurements as well as on double-diffusive heat flux parametrizations. Recent work has shown, however, that in some regions of the Arctic Ocean, the use of a double-diffusive flux parametrization may not be appropriate [e.g., *Carpenter and Timmermans*, 2014]. Planetary rotation, for example, which is not accounted for in double-diffusive flux parametrizations, can reduce double-diffusive heat fluxes expected if the Ekman boundary layer is sufficiently thinner than the interface [*Kelley*, 1987; *Carpenter and Timmermans*, 2014]. If the 4/3 flux parametrization [e.g., *Kelley*, 1990] is appropriate, the parametrized heat flux should equal the molecular heat flux through an undisturbed, laminar interface (measured at its core) in the staircase for density ratios approximately larger than 2 [*Carpenter et al*., 2012; *Sommer et al*., 2013; *Carpenter and Timmermans*, 2014]. *Timmermans et al*. [2008] and *Padman and Dillon* [1987] find that this is the case in the Canada Basin; calculated molecular fluxes from temperature measurements that resolve interfaces were estimated to be approximately 0.2 W m^{-2}, while the parametrization returned comparable values: 0.22 ± 0.10 W m^{-2} [*Timmermans et al*., 2008].

In this paper, we present the first Arctic-wide characterization of the properties of the Atlantic Water Layer thermocline and staircase, relating the staircase structure to the large-scale circulation of the Arctic Ocean. We take advantage of the high-resolution temperature and salinity data from Ice-Tethered Profilers (ITPs) [*Krishfield et al*., 2008a; *Toole et al*., 2011] that sampled over the entire central Eurasian and Canadian Basins. The next section describes the ITP data and analysis methods. In section 3, we characterize the Atlantic Water Layer across the basin by its potential temperature maximum (and salinity and depth at this maximum) and evaluate a bulk vertical density ratio across the depth range of the staircase. In section 4, we examine the details of the staircase structure (layer thicknesses and vertical density ratios across individual layers in the staircase), and identify regions across the Arctic Basin where a staircase structure is present or absent. The validity of a 4/3 flux law parametrization for different regions is examined in section 5, where heat fluxes are also discussed. Finally, in section 6, we summarize and discuss the results.

2. Data and Methods

2.1. Ice-Tethered Profiler Measurements

ITPs measure conductivity, temperature, and pressure in the Arctic water column from several meters below sea ice through the core of the Atlantic Water Layer [*Krishfield et al*., 2008a; *Toole et al*., 2011]. ITPs consist of a surface buoy typically deployed in multiyear sea ice and a wire rope that hangs below to a depth of about 750 m. A profiler supporting a CTD (conductivity-temperature-depth) sensor is mounted on the wire and crawls up and down through the water column (at $\approx$25 cm s^{-1}) two or more times a day. The data (including GPS information) are transmitted by satellite in near real time. A total of approximately 15,800 upgoing profiles from 52 ITPs deployed throughout the Arctic Ocean between 2004 and 2013 are used in the analysis (Figure 2). Note the CTD sensors are located at the top of the profiling unit and measurements made during downgoing profiles are influenced by the wake of the profiler; for the fine-scale structures being examined here, only upgoing profiles are used. Full vertical resolution measurements ($\approx$25 cm for a 1 Hz sampling rate) are used.

The temporal lag between CTD channels is corrected during processing through examination of the temperature-salinity fine structure of the double-diffusive staircase. Temporal lags can often exhibit salinity spikes at the staircase interfaces. Here both the final processed data (Level III) as well as full-resolution Level I data are used. Level I data have only minimum processing applied (i.e., no salinity calibration or lag corrections), while Level III data are fully processed and salinity values are calibrated. Accuracies of temperature and pressure are $\pm$0.001°C and $\pm$1 dbar, respectively. Salinity accuracy is $<$0.005 for the Level III data, and likely worse for the Level I data; however, absolute accuracy does not influence the vertical salinity gradients considered here. Profiles which exhibited salinity spikes from uncorrected sensor response were excluded from the analysis. Full data processing details are in *Johnson et al*. [2007] and *Krishfield et al*. [2008a,2008b] and at www.whoi.edu/itp.

2.2. Characterizing the Thermocline and Double-Diffusive Staircase

We characterize the Atlantic Water Layer by its prominent potential temperature maximum, θ_{max}. Salinity and depth values at the θ_{max} for each profile were also determined. To avoid the selection of spurious

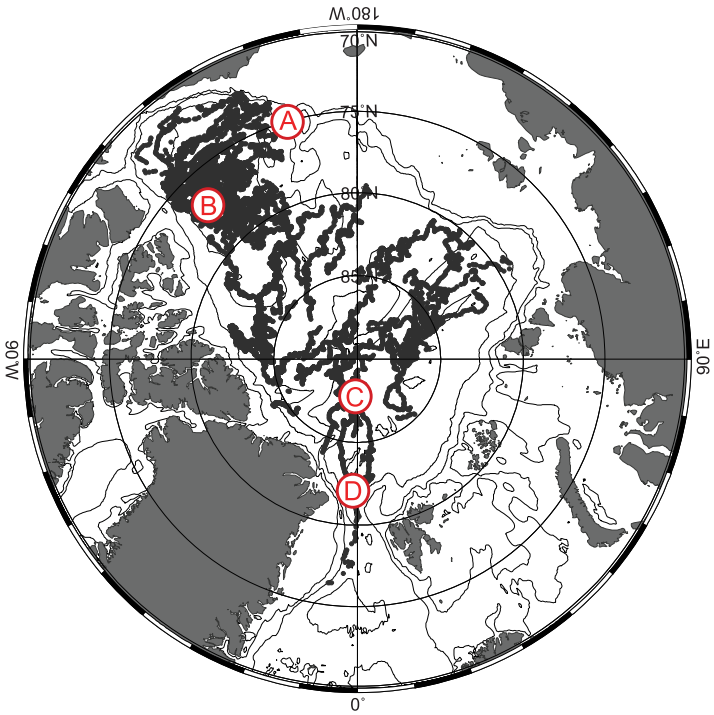

Figure 2. Locations (black dots) of ITP profiles used in this study. ITP upgoing profiles returned between 2004 and 2013 are analyzed here (a total of ≈15,800 ITP profiles with a vertical resolution of ≈25 cm). Red letters (A, B, C, and D) correspond to the profiles shown in Figure 3.

maxima (or potential temperature maxima associated with warm Pacific Water intrusions in the Canadian sector), θ_{max} estimates are restricted to pressures $\geq$ 100 dbar and $<$ 500 dbar, and salinities $\geq$ 34. Profiles where $\theta_{\max} < -1$ °C and $\theta_{\max} > 6$ °C were also excluded from the data set. These criteria were confirmed to exclude only spurious values; further, they are consistent with previous studies indicating $\theta_{max} \approx$ 1–3°C, and the depth at these potential temperature maxima range from about 200–400 m [*Rudels et al.*, 1999; *Timmermans et al.*, 2008; *Lenn et al.*, 2009; *Polyakov et al.*, 2012].

A bulk density ratio, $\overline{R_\rho}$, specifies the relative contributions of the bulk salinity gradient to density and the bulk potential temperature gradient to density as

$$\overline{R_\rho} = \frac{(\beta \Delta S)}{(\alpha \Delta \theta)}, \tag{1}$$

where $\Delta\theta$ and ΔS are vertical potential temperature and salinity changes respectively across some specified depth interval (chosen to be much larger than a typical layer thickness), $\alpha = -\rho_0^{-1}\partial\rho/\partial\theta$ and $\beta = \rho_0^{-1}\partial\rho/\partial S$ are the coefficients of thermal expansion and saline contraction, respectively, ρ is density, and ρ_0 is a reference density. Another characterization of the staircase is via the interface density ratio, R_ρ, which quantifies the relative contributions of the salinity change on density and the potential temperature change on density across each interface in the staircase:

$$R_\rho = \frac{(\beta \delta S)}{(\alpha \delta \theta)}. \tag{2}$$

Both the small-scale R_ρ characterizing individual layers, and the larger-scale bulk $\overline{R_\rho}$, have been calculated in this study.

The depth of the θ_{max} provides a reference point for the choice of an appropriate depth range across which to characterize the staircase. A specified depth above the Atlantic Water Layer θ_{max} that indicated a deep bound on the staircase region was visually identified for each ITP (with the exception of ITP 56 drifting in the Eurasian Basin, where two bounds were determined on either side of warm fronts). The deep bound was selected to avoid the interleaving intrusions that are generally found in depths around the core of the Atlantic Water Layer [e.g., *Walsh and Carmack*, 2003]. For ITPs that drifted in the Eurasian Basin, this bound was 106 $\pm$ 23 m above the Atlantic Water Layer θ_{max}, and in the Canadian Basin was 142 $\pm$ 13 m above the Atlantic Water Layer θ_{max}. An interval of 50 m above the deep bound was then used for the determination of bulk water-column properties in the staircase region.

Four representative profiles from (a) the boundary of the Canada Basin, (b) the central Canada Basin, (c) the Eurasian Basin, and (d) the vicinity of Fram Strait indicate how the appropriate depth range changes from region to region (Figure 3; locations are shown in Figure 2). The bulk density ratio, $\overline{R_\rho}$, was computed based on bulk potential temperature and salinity gradients (from end-point differences) over these 50 m depth intervals; α and β were computed at the mid-depth of the interval. Any value of $\overline{R_\rho}$ greater than 10 or less than 1 was excluded. Close inspection of the profiles indicated that values in these ranges were associated

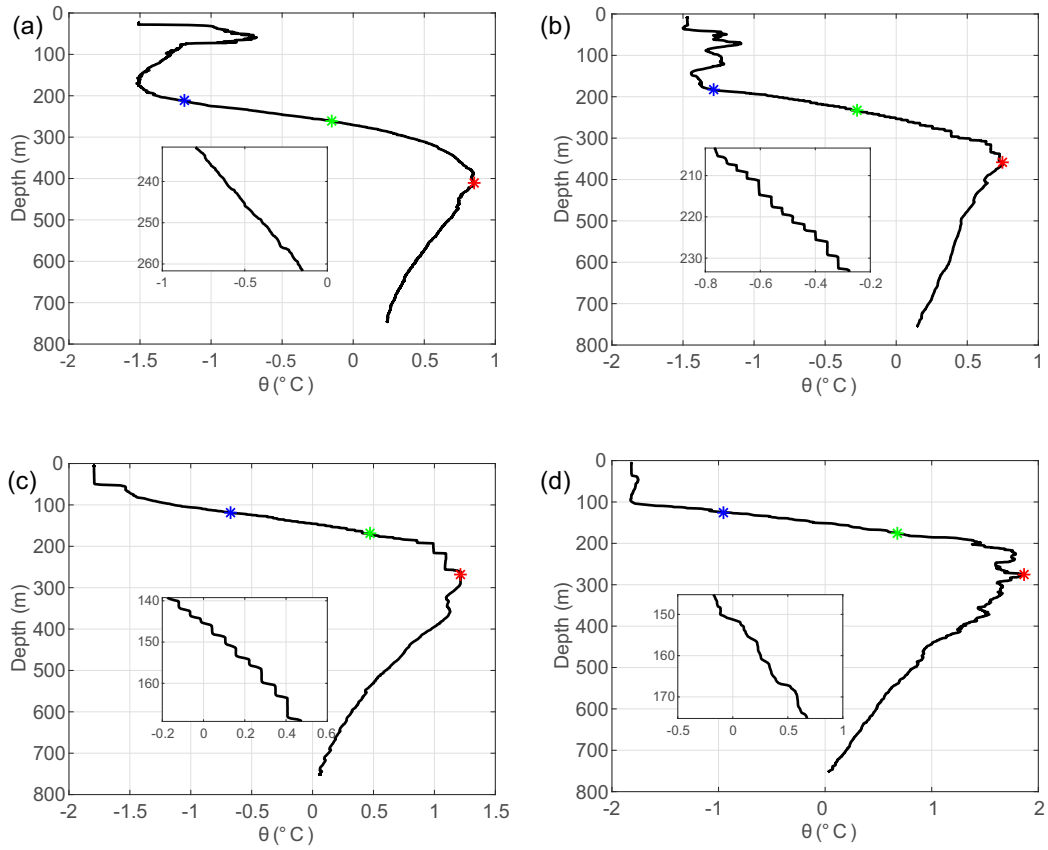

Figure 3. Four representative profiles of potential temperature (°C) (locations marked in Figure 2): (a) at the boundary of the Canadian Basin (A: ITP 8, 23 May 2009), (b) from the central Canadian Basin (B: ITP 1, 26 Jun 2006), (c) in the Eurasian Basin (C: ITP 56, 29 May 2012), and (d) in the vicinity of Fram Strait (D: ITP 7, 29 Sep 2007), indicate the appropriate thermocline region in various regions of the Arctic Basin. Given these differences, in order to properly quantify the double-diffusive staircase, a unique deep bound of the 50 m staircase interval (marked by green stars for the profiles shown) was determined for each ITP. Blue stars delineate the shallow bound. The red star indicates the Atlantic Water Layer θ_{max} in each profile. Insets in each plot show a zoom-in of the potential temperature profile in the 50 m depth interval.

with spurious temperature and/or salinity measurements or isolated mischaracterization of the double-diffusive staircase interval, which can occur by selecting a depth interval (with too shallow an upper bound, for example) over which the gradient can no longer be considered linear.

Our algorithm for characterizing the double-diffusive staircase on an Arctic-wide scale expands on that described by *Timmermans et al.* [2008]; *Timmermans et al.* [2008] only consider the staircase in a specific region of the Canada Basin. The lower 25 m of each 50 m depth segment for a given profile was taken as the depth interval to characterize individual layers and interfaces in the staircase. Layers are consistently most prominent in this range (layer thickness tends to increase with depth). While the depth interval of 50 m is best for the calculation of $\overline{R_\rho}$ (a smaller depth interval may be influenced by individual layers), we find that $\overline{R_\rho}$ calculated over the lower 25 m is smaller than $\overline{R_\rho}$ calculated over 50 m by less than 15%. Layers in the staircase are taken to lie where the potential temperature difference between two adjacent data points in a profile was less than a threshold value (between 0.001 and 0.006°C), which was determined to be most appropriate (by trial and visual inspection) for each ITP. The potential temperature gradient $\partial\theta/\partial z$ in a layer was required to be less than a second threshold value (between 0.001 and 0.009°C m^{-1}) which was also determined for each ITP. The detection of at least three layers, not including the first and last layer (that may have been only partially sampled), and a sum of layer depths of at least 6.25 m, were required to mark a staircase as present in that profile. The minimum requirement of 6.25 m ensures that a significant portion (at least 25%) of the depth interval is occupied by layers. Mean layer thickness, $\bar{h}$, was calculated by averaging the thicknesses of layers in each profile, excluding the first and last layers in the 25 m segment. Approximately 3600 mixed layers in the Eurasian Basin and 75,600 mixed layers in the Canadian Basin have

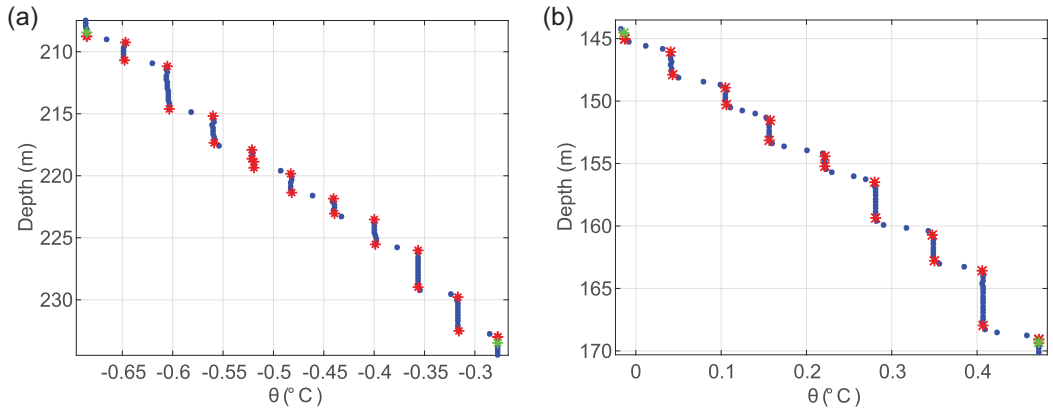

Figure 4. Potential temperature, θ (°C), profiles in the staircase region in (a) the Canadian Basin and (b) the Eurasian Basin. Interfaces are too thin to be resolved in the Canadian sector. Interfaces may be resolved with ITP measurements in the Eurasian sector, as more data points tend to be returned between layers than in the Canadian Basin. Blue dots indicate ITP data points approximately every 25 cm. Green stars indicate the beginning and end of the staircase region, while red stars indicate the top and bottom of respective layers.

been analyzed in this study. The density ratio, R_ρ, was computed over individual interfaces using the values of $\delta\theta$ and δS between adjacent layers.

Atlantic Water Layer staircase interface thicknesses, δh, have been described previously in various sectors of the Arctic Basin. There is a large range of δh reported in the literature. *Polyakov et al.* [2012] estimate interface thicknesses in the Laptev Sea of $1 < \delta h < 5$ m, and *Padman and Dillon* [1989] find $\delta h \approx 0.15$ m in the Canada Basin. Given these measurements and estimates, and the limiting vertical ITP resolution of 0.25 m, interfaces generally tend to be too thin in the Canadian sector to be resolved with the ITP measurements (Figure 4). Where interfaces are too thin to be resolved by ITP measurements, it remains possible to infer heat fluxes using a double-diffusive flux law parametrization, provided we can rely on the verification of past studies that such a flux law is appropriate in the region in question. We discuss these parametrized heat fluxes further in section 5.

For the thicker interfaces in the Eurasian Basin, interfaces were identified as the regions between adjacent layers (the thickness between the top of one layer and the bottom of that adjacent). If the interface was thicker than a threshold value, which was determined by inspection for each ITP (and taken to be between 1.75 and 2.5 m), it was excluded from the analysis of interfaces. (Interfaces thicker than this limit tended to include mixed layers that had not been identified in our algorithm.) If at least two interfaces were present in a staircase region, the mean interface thickness, $\overline{\delta h}$, was calculated for the profile. Approximately 3100 interfaces have been analyzed. We corroborate our interface thickness calculations by comparing the mean interface thickness for a profile to the median interface thickness for a profile. Across the Eurasian Basin, these values vary by less than 5% (i.e., spurious anomalously thick interfaces are not significantly biasing the values). In section 4, we quantify the uncertainty associated with the finite vertical resolution of ITP measurements.

2.3. Heat Fluxes

The main motivation for investigating the double-diffusive staircase is for its relevance to vertical heat fluxes from the Atlantic Water Layer to the overlying water layers. Typically, heat fluxes through double-diffusive staircases are computed using parametrizations formulated by empirical fits to laboratory and oceanographic data. One of the most commonly used double-diffusive parametrizations for the heat flux (in W m^{-2}) is given by *Kelley* [1990]:

$$F_H = 0.0032 e^{4.8/R_\rho^{0.72}} \rho c_p \left(\frac{\alpha g \kappa}{Pr}\right)^{1/3} (\delta\theta)^{4/3}, \tag{3}$$

where c_p is the specific heat of water, $\kappa \approx 1.4\times10^{-7}$ m^2 s^{-1} is the molecular diffusivity of heat, g is gravity, and $Pr = \nu/\kappa$ is the Prandtl number, where $\nu \approx 1.8\times10^{-6}$ m^2 s^{-1} is the kinematic viscosity. The value of this formalism is that only the temperature jump across a double-diffusive interface must be resolved, and not the interface thickness (which is often too thin to be resolved without microstructure measurements). In regions where interfaces can be resolved, a molecular heat flux F_M can be computed across an undisturbed, laminar

interface core, $F_M = \rho c_p \kappa \frac{\partial \theta}{\partial z}$. A reasonable check as to the validity of the 4/3 flux parametrization in this region can be made by comparing the magnitudes of F_M and F_H; we discuss this further in section 5.

3. Bulk Properties of the Atlantic Water Layer

The Atlantic Water Layer θ_{max}, salinity of the θ_{max}, depth of the θ_{max}, $\overline{R_\rho}$, and $\bar{h}$ show significant spatial variability across the Arctic Basin over the study period. In contrast, temporal variability in Atlantic Water Layer properties appears to be negligible. The Atlantic Water Layer typically exhibits much smaller seasonal and interannual variability than surface waters more directly influenced by seasonally varying surface buoyancy fluxes and wind-driven variability. We observe that in the Canadian Basin, the θ_{max} changes at a rate of -0.02 ± 0.16°C per year (over 2004–2013), and in the Eurasian Basin, the θ_{max} changes at a rate of -0.01 ± 0.30°C per year (i.e., there is no statistically significant trend in either of the two main basins over the decade of ITP measurements). The spatial difference in θ_{max} over a section from the Eurasian to Canadian Basins (44°E, 85°N to 135°W, 72°N) is around 2°C. Thus, we make the assumption that temporal variations of the basin waters may be neglected relative to the spatial variations, and we consider the large-scale spatial patterns presented here to be effectively synoptic.

3.1. Properties of the Atlantic Water Layer θ_{max}

As the Atlantic Water enters the Arctic Basin and circulates eastward into the Canadian Basin, heat is lost through turbulent ocean mixing with cooler waters (as well as wind-driven upwelling onto shallow shelves and surface buoyancy fluxes) and also through double-diffusive heat fluxes. The Atlantic Water Layer is appreciably cooler in the Canadian Basin, where $\theta_{max} \approx 0.73$°C, compared to the Eurasian Basin, where $\theta_{max} \approx 1.30$°C (Figure 5a). The Atlantic Water Layer θ_{max} is coldest in the northeast Canadian Basin off the coast of Ellesmere Island. Here the waters have propagated cyclonically over the full extent of the Arctic Basin. Maximum and minimum observed θ_{max} are 4.10°C and -0.68 °C, respectively (Figure 5a).

The Atlantic Water Layer salinity at θ_{max} is highest closest to the inflow region and freshens following the decrease in θ_{max}, again because of turbulent mixing with overlying fresher waters and double-diffusive salt fluxes as the Atlantic Water Layer circulates the basin (Figure 5b). The Atlantic Water Layer core is shallowest near Fram Strait (approximately 200 m deep) and increases (by mixing processes and downwelling) along the cyclonic pathway with maximum depths found in the central Beaufort Gyre region (approximately 440 m deep), where deepening of isopycnals arises as a result of the large-scale anticyclonic wind forcing [*Proshutinsky et al.*, 2009] (Figure 5c).

3.2. The Bulk Density Ratio $\overline{R_\rho}$

The bulk density ratio, $\overline{R_\rho}$, is lowest in boundary regions of the Eurasian Basin, where the Atlantic Water Layer core is warmest (Figure 5d). In the Eurasian Basin, $\overline{R_\rho} = 4.0 \pm 1.3$. $\overline{R_\rho}$ increases along the cyclonic pathway of the Atlantic Water Layer around the Arctic Basin, and takes values of $\overline{R_\rho} = 6.3 \pm 1.4$ in the Canadian Basin. Low values of $\overline{R_\rho}$ near the Atlantic Water inflow region are best described by larger vertical potential temperature gradients than in other regions; in general, larger bulk temperature gradients in the staircase are associated with larger θ_{max}. The largest values of $\overline{R_\rho}$ are found in the regions of coolest Atlantic Water Layer θ_{max}, where the bulk potential temperature gradient through the staircase is smallest (Figure 6a). Unlike the bulk potential temperature gradient across the staircase (and therefore θ_{max}), variations in the bulk salinity gradient across the staircase show no clear spatial pattern.

Values of $\overline{R_\rho}$ show an approximately bimodal distribution, with peaks at approximately 3 and 6, corresponding to values in the Eurasian and Canadian Basins, respectively (Figure 6b). The second, smaller peak above $\overline{R_\rho} \approx 6$ appears to be associated with the slightly higher values in the northeastern Canadian Basin. These differences in $\overline{R_\rho}$ are manifest in the differing slopes of θ-S plots (in the region of the staircase) of representative profiles in the respective basins (shown in Figure 1c).

4. Staircase Properties

4.1. Presence or Absence of Layers

A well-defined staircase exists throughout most of the central Arctic Basin but is generally not observed in the Eurasian Basin and along boundaries near the Atlantic Water inflow (Figure 7a). It is unclear whether

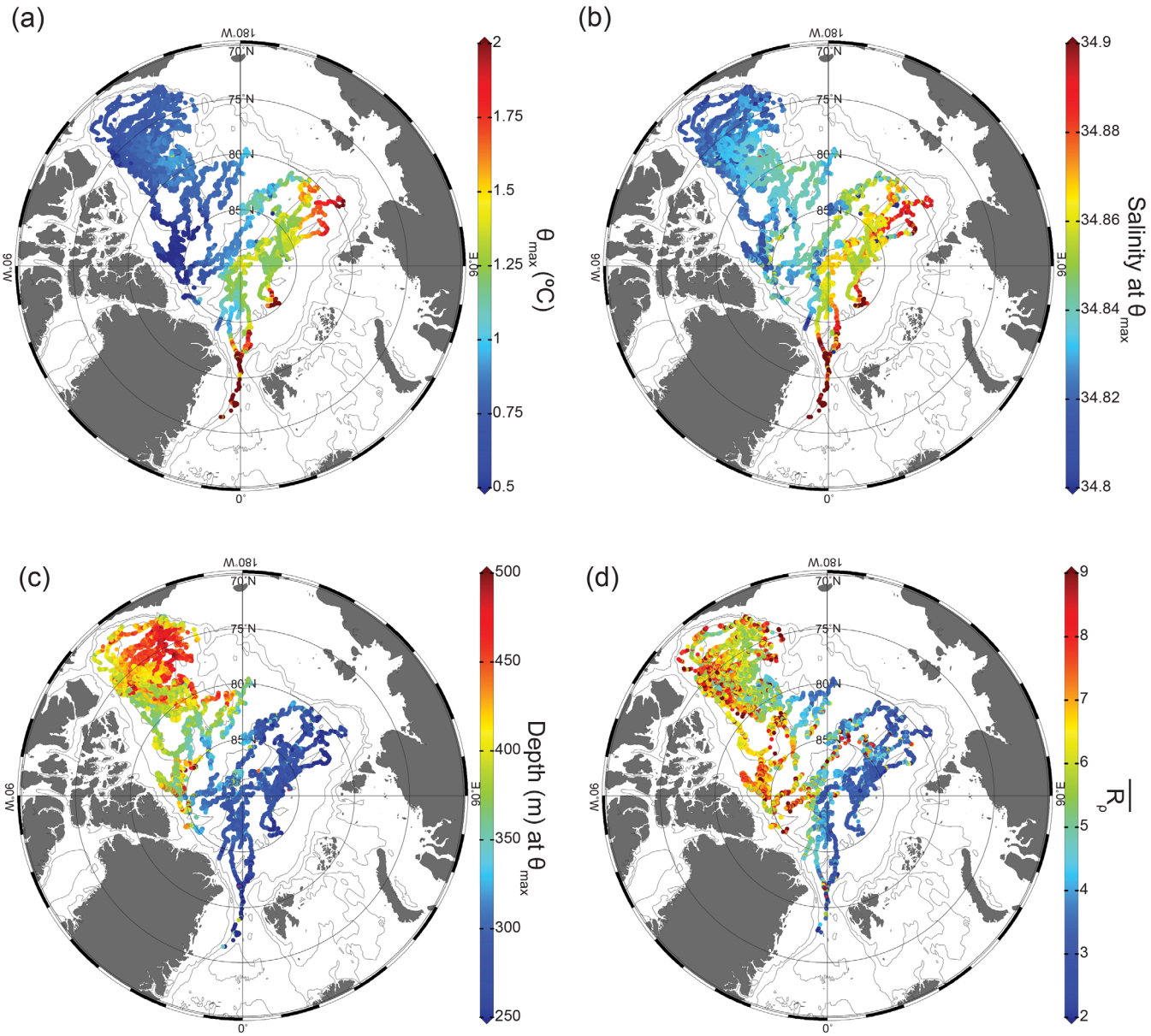

Figure 5. (a) Map of θ_{max} (°C) across the Arctic Basin. (b) Map of salinity at θ_{max}. (c) Map of depth (m) at θ_{max}. (d) Map of $\overline{R_\rho}$. As Atlantic Water circulates around the basin, its core θ_{max} and salinity at core θ_{max} decrease, while its depth at core θ_{max} and $\overline{R_\rho}$ increase.

this is due to the dominance of turbulent mixing over double diffusion. In the Eurasian Basin, the Atlantic Water Layer thermocline is closer to the surface and less sheltered by the overlying stratification from winds and surface buoyancy forcing. The distribution of a staircase structure (Figure 7a) provides a conservative estimate, with profiles marked as having no staircase if the criterion described in section 2.2 is not satisfied. Only approximately 24% of profiles in the Eurasian Basin and in the vicinity of Fram Strait indicate a staircase, as compared to 80% in the Canadian Basin. Boundary regions are generally characterized by fewer, thinner layers, and the 25 m region over which layers were examined often does not exhibit a staircase structure over the entire interval. It is possible that in these boundary regions, layers have had less time to merge and thicken [e.g., *Radko*, 2007], potentially unlike layers in the interior of the Arctic.

4.2. Layer Thicknesses and Interface Properties

Mean layer thicknesses, $\overline{h}$, are generally in the range 0.5–3.5 m, with similar values between the Canadian Basin and Eurasian Basin (Figures 7b and 8); the thin bound is set by the vertical resolution of the

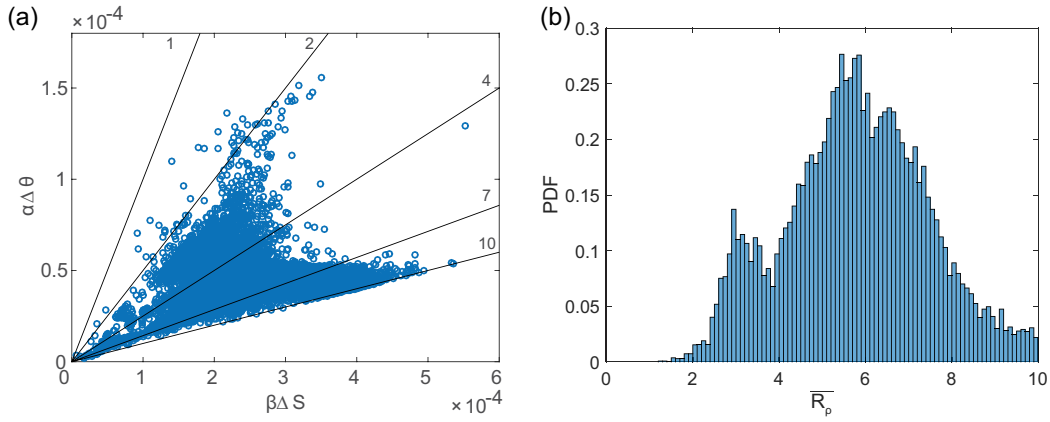

Figure 6. (a) Scatterplot of $\alpha\Delta\theta$ versus $\beta\Delta S$ with contours of $\overline{R_\rho}$ overlain. Large values of $\overline{R_\rho}$ (appearing as a lower branch in the plot) are found in the Canadian Basin, while low values of $\overline{R_\rho}$ (upper branch) are found in the Eurasian Basin. (b) PDF of $\overline{R_\rho}$ for all profiles. The two main peaks (with $\overline{R_\rho} \approx 3$ and $\overline{R_\rho} \approx 6$) generally correspond to the Eurasian Basin and the Canadian Basin, respectively. The greater density of $\overline{R_\rho} \approx 6$ observations (compared to those with $\overline{R_\rho} \approx 3$) is a result of more ITP profiles in the Canadian Basin. The bin width is 0.1.

measurements. Across the entire Arctic Ocean, mean layer thicknesses do not exhibit a spatial pattern, and so we cannot relate $\bar{h}$ to the large-scale circulation. On the other hand, $\overline{\delta\theta}$ across interfaces appears to be related to the large-scale circulation, as $\overline{\delta\theta}$ is on average higher in the Eurasian Basin than in the Canadian Basin (Figures 8 and 9a), following a similar pattern to θ_{max} and $\Delta\theta$ across the 50 m staircase region. $\overline{\delta S}$ across interfaces takes similar values in the Eurasian and Canadian Basins, though several high values are found in the eastern Canadian Basin (Figures 8 and 9b), where θ_{max} is smallest. The spatial patterns of $\overline{\delta\theta}$ and $\overline{\delta S}$ parallel those of $\Delta\theta$ and ΔS, and thus we find similar patterns between mean interface R_ρ (not shown) and bulk $\overline{R_\rho}$ (Figure 5d), although with slight differences that could be due to curvature in the thermocline gradient over the depth interval of interest, or to layers not being precisely resolved. In the Canada Basin, *Timmermans et al*. [2008] find similar correspondence between R_ρ and $\overline{R_\rho}$, with R_ρ calculated over individual layers varying between 2 and 7 and bulk $\overline{R_\rho}$ values in the same region varying between 3 and 6. In the Eurasian Basin, the distribution of R_ρ (Figure 8) is similar to that described by *Guthrie et al*. [2015].

It is also of interest to compute the Rayleigh number, $\overline{Ra} \equiv g\alpha\overline{\delta\theta}\bar{h}^3/\nu\kappa$ for each mixed layer, since the term $(\delta\theta)^{4/3}$ in the 4/3 flux law (e.g., Kelley's parametrization) originates from the relationship between the Rayleigh number and the ratio of convective to conductive heat flux [*Turner*, 1965]. The Rayleigh number describes the relative effects of the thermal buoyancy forcing to viscosity and diffusion across an interface. We find similar values of $log_{10}\overline{Ra}$ between the Eurasian and Canadian Basins (Figure 8), indicating comparable effects of thermal forcing to viscosity and diffusion between basins. The distribution of $\overline{Ra}$ in the Eurasian Basin is similar to that described by *Guthrie et al*. [2015].

Finally, in the Eurasian Basin, where interfaces may be sufficiently thick to be resolved by ITP profiles, values of mean interface thickness, $\overline{\delta h}$, generally fall between 0.5 and 2 m (Figures 7c and 8). Based on an approximate vertical measurement resolution of 25 cm, interfaces may be up to 0.5 m thinner than inferred by ITP measurements. For the majority of interfaces measured in the Eurasian Basin (99% range from 0.5 to 2.0 m), the maximum percent uncertainty in thickness ranges from 100% to 25%. There are profiles, however, for which the vertical resolution is better than every 25 cm; while the sample rate remains the same, there is some variation in ITP profiling speed. It is instructive to consider how the varying vertical resolution of ITP profiles in the Eurasian Basin relates to the inferred interface thickness. Mean resolution for a given profile is calculated by averaging the depth differences between adjacent samples from the top of the staircase region to the depth of the Atlantic Water Layer θ_{max}. There exists a positive, linear relationship between mean inferred interface thickness $\overline{\delta h}$ and binned 5 cm mean resolution (Figure 10a). There are only relatively few profiles with improved resolution (in cases where ITP profiling speed was slower than the mean), and it is not possible to conclude to what extent profile resolution biases inferred interface thickness statistics. We thus consider this potential error in our calculations of molecular heat fluxes.

The mean $\overline{\delta h}$ of all profiles (at any vertical resolution) in the Eurasian Basin is 1.1 m (Figure 8). These measurements contrast with *Guthrie et al*. [2015], who find an average interface thickness of 0.1 m for interfaces

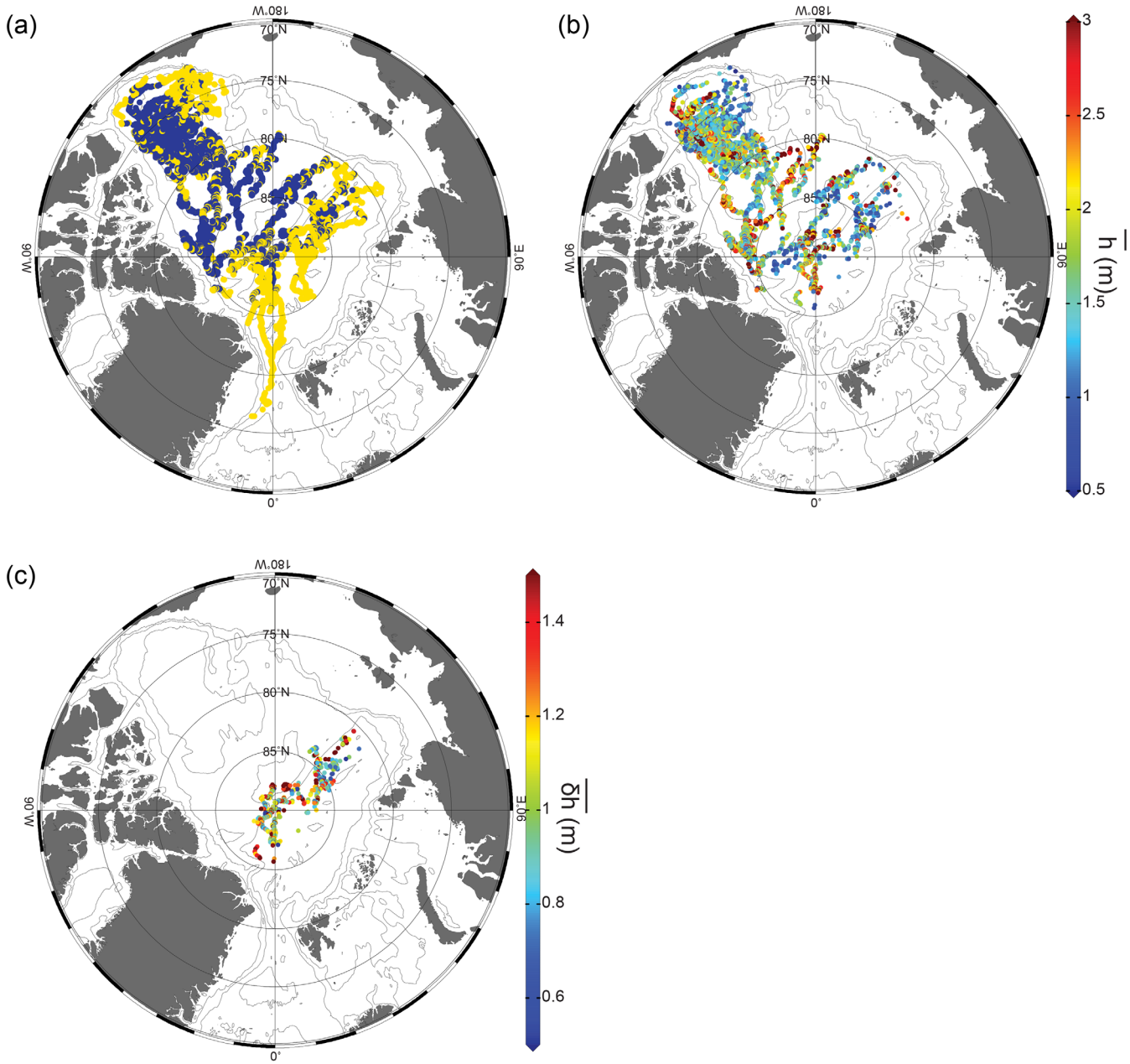

Figure 7. (a) Map indicating presence (blue) or absence (yellow) of a well-defined double-diffusive staircase. Well-defined layers exist throughout the majority of the central Arctic Basin, with an absence of layers most pronounced in the Eurasian Basin. (b) Map of mean layer thickness, $\overline{h}$ (m), indicating no apparent spatial pattern. (c) Map of mean interface thickness, $\overline{\delta h}$ (m). Interface thicknesses in the Eurasian Basin do not exhibit a distinctive pattern.

in the Amundsen Basin, with values ranging from slightly larger than 0 to 0.4 m. These low values may be due in part to the fact that *Guthrie et al.* [2015] find very thin mixed layers sandwiched within interfaces, which can make one thick interface appear as at least two thinner interfaces (see their Figure 10). However, it is difficult to know whether these thin layers found between interfaces are actually in steady state or are short-lived turbulent overturns that occur in general for $R_\rho < 3$ [e.g., *Sommer et al.*, 2014]; in some circumstances, instrument noise may also be a factor [see e.g., *Johnson and Garrett*, 2004]. Over an ITP transect (from ITP 38) similar to the region of interest in *Guthrie et al.* [2015], we find mean interface $R_\rho < 3$ for over 60% of the profiles; this raises the possibility that the large number of values near 0 m in the histogram of mixed layer thickness in *Guthrie et al.* [2015, Figure 3] may actually be these turbulent disturbances within interfaces. We also observe these features in a similar region of the Amundsen Basin in ITP 38 profiles

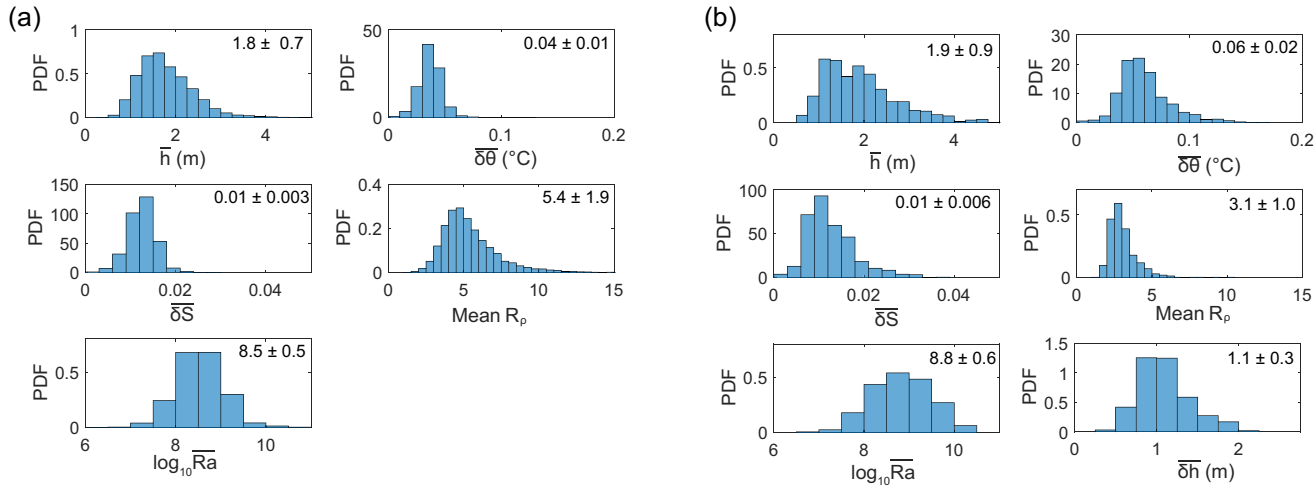

Figure 8. PDFs of $\bar{h}$ (m), $\overline{\delta\theta}$ (°C), $\overline{\delta S}$, mean interface R_ρ over a profile (distinct from $\overline{R_\rho}$), $\overline{Ra}$, and $\overline{\delta h}$ (m) in (a) the Canadian Basin and (b) the Eurasian Basin. Bin sizes are 0.25 m, 0.01°C, 0.003, 0.5, 0.5, and 0.25 m, respectively. The mean value (±1 standard deviation) is given on each plot. Approximately 75,600 mixed layers are analyzed in the Canadian Basin. Approximately 3600 mixed layers and 3100 interfaces are analyzed in the Eurasian Basin.

(Figure 10b). This uncertainty in interface thickness is taken into account in our assessment of heat fluxes in section 5.

5. Heat Fluxes

Previous studies have shown that laboratory flux laws agree with observed heat fluxes in the Canadian Basin [*Padman and Dillon*, 1987; *Timmermans et al.*, 2008]. Applying the parametrization (3) to the ITP data, we derive heat fluxes of O(0.1) W m^{-2} for this region (Figure 11); it should be noted that for $R_\rho \gtrsim 3$, *Flanagan et al.* [2013] find through numerical experiments that fluxes parametrized by the 4/3 flux law of *Kelley* [1990] may be underestimated by up to about 50%. Highest fluxes are found near the eastern boundary of the Lomonosov Ridge, consistent with where the Atlantic Water Layer is warmest in the Canadian Basin where it enters from the Eurasian Basin. It is of note that the distribution of heat in the Canadian Basin is somewhat more complicated than would be inferred from a direct cyclonic pathway of the Atlantic Water; the separation of the Atlantic Water Layer from the vicinity of the Northwind Ridge and its eastward

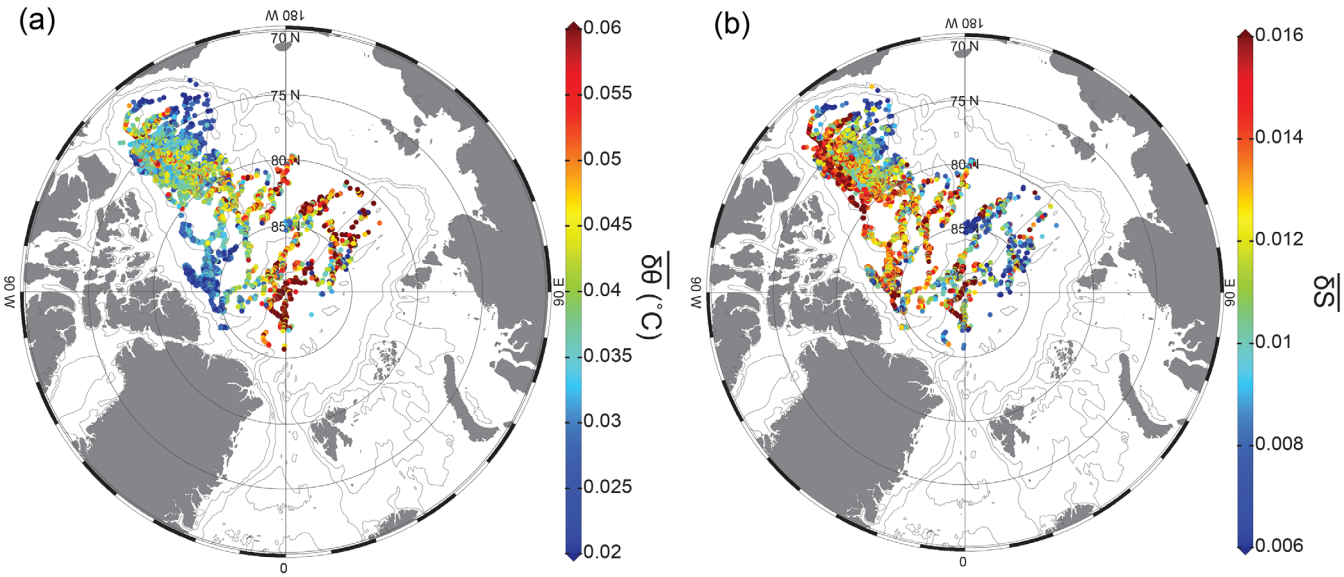

Figure 9. (a) Map of mean potential temperature difference across interfaces, $\overline{\delta\theta}$ (°C). (b) Map of mean salinity difference across interfaces, $\overline{\delta S}$.

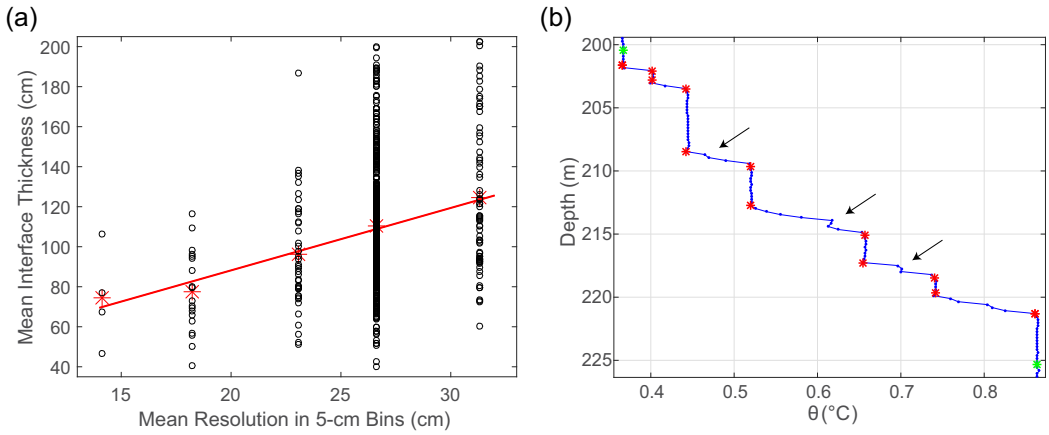

Figure 10. (a) Mean interface thickness $\overline{\delta h}$ for profiles in the Eurasian Basin versus mean vertical measurement resolution in 5 cm bins. Black circles show the values of $\overline{\delta h}$ for each profile with red stars indicating the mean for a given resolution bin. There exists a positive, linear relationship ($R^2 = 0.97$) between inferred interface thickness and mean resolution. Mean resolution is calculated per profile by averaging the depth differences between adjacent samples from the top of the staircase region to the depth of the θ_{max}. (b) Potential temperature (°C) profile from the Amundsen Basin (ITP 38). Green stars indicate the start and end of the 25 m depth interval over which the staircase is characterized. Red stars mark the boundaries of interfaces. Small blue dots indicate measurements taken from the ITP. The vertical measurement resolution of this profile is 24 cm. Possible unresolved mixed layers or overturns are exhibited in some interfaces (indicated by arrows).

penetration into the central basin [*McLaughlin et al.*, 2004] is consistent with the large values of heat flux found in the central Beaufort Gyre.

In the Eurasian Basin, we attempt to examine the validity of the 4/3 flux law; for this we can compare the magnitudes of F_M and F_H if the interfaces have been resolved. For example, for values of $\delta\theta$ in the Eurasian Basin, application of Kelley's 4/3 flux law yields a mean heat flux of 0.7 ± 0.4 W m^{-2}. To support a molecular heat flux of this magnitude, interfaces would need to be as thin as 0.08 ± 0.05 m. However, ITP measurements indicate they are typically a little more than 1 m thick (Figure 4b). It is possible that due to the thicker interfaces, rotation plays an important role in double-diffusive convection here, which is not accounted for in Kelley's 4/3 flux parametrization [*Kelley*, 1987; *Carpenter and Timmermans*, 2014]. This could be the case since the Ekman layer thickness of a laminar interface ($\approx$0.1 m for the Eurasian Basin) is significantly smaller than the interface thickness [*Carpenter and Timmermans*, 2014]. On the other hand, we cannot rule out the presence of small layers within what we are taking to be the thicker Eurasian Basin interfaces given the relatively coarse resolution of the profiles, in which case a 4/3 flux parametrization may apply. In the event that the interfaces are split by a single mixed layer, we would obtain double-diffusive fluxes based on the parametrization in *Kelley* [1990] that are 60% lower than would otherwise be obtained; a mean heat flux of 0.7 ± 0.4 W m^{-2} based on the 4/3 flux law in the Eurasian Basin would be reduced to 0.3 ± 0.2 W m^{-2}.

By computing the molecular heat flux (averaged per profile) through each interface using the change in potential temperature across each interface and the interface thickness inferred from ITP measurements, we find heat fluxes of O(0.01) W m^{-2} in the Eurasian Basin. Given the resolution of the profilers, these interfaces may be overestimated by as much as 0.5 m; if this is the case, molecular heat fluxes could be as large as O(0.1) W m^{-2}. It is also important to note that the low values of $\overline{R_\rho}$ in the Eurasian Basin may imply that the interfaces are disturbed by turbulence; therefore, actual fluxes could be larger than the F_M estimates.

6. Summary and Discussion

While there have been previous studies of the double-diffusive staircases in specific regions of the Arctic, this is the first study to examine the Arctic thermocline staircase on a basin-wide scale. This Arctic-wide analysis allows us to examine where double-diffusive flux laws may or may not be valid as well as hypothesize about what factors influence the presence or absence of staircase features in particular regions. Properties of the Atlantic Water Layer and double-diffusive staircase at its top boundary have been

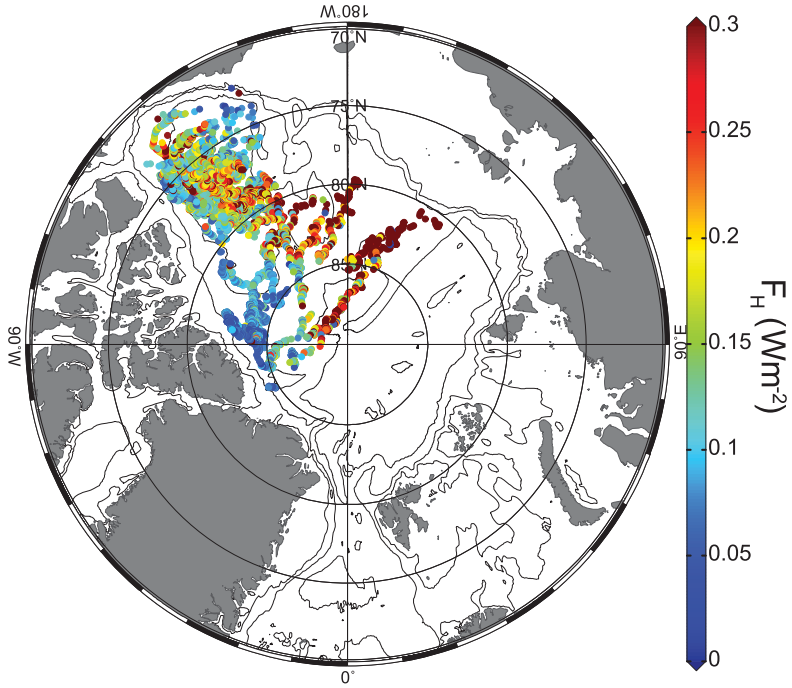

Figure 11. Heat fluxes (W m^{-2}) in the Canadian Basin (computed using the 4/3 flux law); fluxes are O(0.1) W m^{-2}, with the highest values near the eastern Lomonosov Ridge.

analyzed using ITP data from across the Arctic Basin collected between 2004 and 2013; this study takes advantage of the ITP data sampling the detailed structure of the thermohaline staircase laterally across the entire Arctic. As Atlantic Water circulates around the Arctic Basin, its maximum core potential temperature and salinity decrease, as expected. The bulk density ratio, $\overline{R_\rho}$, is lowest in regions of the Eurasian Basin where the Atlantic Water Layer is warmest, and increases along the cyclonic pathway of the Atlantic Water Layer around the Arctic Basin. There is no apparent relationship between $\overline{R_\rho}$ and staircase layer thicknesses across the basin. Well-defined layers exist throughout the majority of the central Arctic Basin, while an absence of layers is most pronounced in the Eurasian Basin and in the vicinity of Fram Strait. It is not known whether the lack of a staircase structure is due to the dominance of turbulent mixing over double diffusion (see, e.g., *Rippeth et al*. [2015] who demonstrate generally higher turbulent mixing levels at basin boundaries in the Arctic). Furthermore, in the absence of a double-diffusive flux to maintain the staircase structure, staircases would not persist very long: an interface would increase in thickness by molecular conduction alone by about 20 cm in 1 day, thereby smoothing out the profile and reducing the distinct staircase structure.

In the Canadian Basin, using a double-diffusive 4/3 flux law parametrization, the distribution of vertical heat fluxes through the staircase is estimated to be O(0.1) W m^{-2}. It is questionable whether the 4/3 flux law yields an appropriate representation of heat fluxes in the Eurasian Basin. We estimate molecular heat fluxes in the Eurasian Basin to be between O(0.01) and O(0.1) W m^{-2}; *Polyakov et al*. [2012] and *Guthrie et al*. [2015] report parametrized heat fluxes of O(0.1) to O(1) W m^{-2} for the region (note that the high heat fluxes inferred by *Polyakov et al*. [2012] are over the Laptev Sea slope where we do not have measurements). However, it is unclear if Eurasian Basin heat fluxes are well represented by a laminar molecular heat flux calculation at such low $\overline{R_\rho}$. The discrepancy in heat fluxes between the two basins is counterintuitive, as fluxes in the Eurasian Basin are smaller (subject to many uncertainties) where the source water is warmer. Future work will investigate possible explanations for this discrepancy.

Further questions remain as to the transition from laminar to turbulent interfaces. Future work will compare DNS results of heat fluxes with measured ocean heat fluxes to determine the limitations of 4/3 flux parametrizations at low $\overline{R_\rho}$. Additional data at higher vertical resolution are necessary for closer inspection of interfaces in the Eurasian Basin.

Acknowledgments
The Ice-Tethered Profiler data were collected and made available by the Ice-Tethered Profiler Program [*Krishfield et al.*, 2008a; *Toole et al.*, 2011] based at the Woods Hole Oceanographic Institution (http://www.whoi.edu/itp). Funding was provided by the National Science Foundation Division of Polar Programs under award 1350046.

References

Aagaard, K., L. Coachman, and E. Carmack (1981), On the halocline of the Arctic Ocean, *Deep Sea Res., Part A*, *28*(6), 529–545, doi:10.1016/0198-0149(81)90115-1.

Carmack, E., et al. (2015), Toward quantifying the increasing role of oceanic heat in sea ice loss in the new Arctic, *Bull. Am. Meteorol. Soc.*, *96*(12), 2079–2105, doi:10.1175/BAMS-D-13-00177.1.

Carpenter, J., and M.-L. Timmermans (2014), Does rotation influence double-diffusive fluxes in polar oceans?, *J. Phys. Oceanogr.*, *44*(1), 289–296, doi:10.1175/JPO-D-13-098.1.

Carpenter, J., T. Sommer, and A. Wüest (2012), Simulations of a double-diffusive interface in the diffusive convection regime, *J. Fluid Mech.*, *711*, 411–436, doi:10.1017/jfm.2012.399.

Fer, I. (2009), Weak vertical diffusion allows maintenance of cold halocline in the central Arctic, *Atmos. Oceanic Sci. Lett.*, *2*(3), 148–152, doi:10.1080/16742834.2009.11446789.

Flanagan, J. D., A. S. Lefler, and T. Radko (2013), Heat transport through diffusive interfaces, *Geophys. Res. Lett.*, *40*, 2466–2470, doi:10.1002/grl.50440.

Guthrie, J. D., I. Fer, and J. Morison (2015), Observational validation of the diffusive convection flux laws in the Amundsen Basin, Arctic Ocean, *J. Geophys. Res. Oceans*, *120*, 7880–7896, doi:10.1002/2015JC010884.

Johnson, G. C., J. M. Toole, and N. G. Larson (2007), Sensor corrections for sea-bird SBE-41CP and SBE-41 CTDs, *J. Atmos. Oceanic Technol.*, *24*(6), 1117–1130, doi:10.1175/JTECH2016.1.

Johnson, H. L., and C. Garrett (2004), Effects of noise on Thorpe scales and run lengths, *J. Phys. Oceanogr.*, *34*(11), 2359–2372, doi:10.1175/JPO2641.1.

Kelley, D. (1987), The influence of planetary rotation on oceanic double-diffusive fluxes, *J. Mar. Res.*, *45*(4), 829–841, doi:10.1357/002224087788327136.

Kelley, D. (1990), Fluxes through diffusive staircases: A new formulation, *J. Geophys. Res.*, *95*(C3), 3365–3371, doi:10.1029/JC095iC03p03365.

Kelley, D., H. Fernando, A. Gargett, J. Tanny, and E. Özsoy (2003), The diffusive regime of double-diffusive convection, *Prog. Oceanogr.*, *56*(3-4), 461–481, doi:10.1016/S0079-6611(03)00026-0.

Krishfield, R., J. M. Toole, A. Proshutinsky, and M.-L. Timmermans (2008a), Automated Ice-Tethered Profilers for seawater observations under pack ice in all seasons, *J. Atmos. Oceanic Technol.*, *25*(11), 2091–2105, doi:10.1175/2008JTECHO587.1.

Krishfield, R., J. M. Toole, and M.-L. Timmermans (2008b), ITP data processing procedures, technical report, Woods Hole Oceanogr. Inst., Woods Hole, Mass.

Lenn, Y.-D., et al. (2009), Vertical mixing at intermediate depths in the Arctic boundary current, *Geophys. Res. Lett.*, *36*, L05601, doi:10.1029/2008GL036792.

Maykut, G. A., and N. Untersteiner (1971), Some results from a time-dependent thermodynamic model of sea ice, *J. Geophys. Res.*, *76*(6), 1550–1575, doi:10.1029/JC076i006p01550.

McLaughlin, F., E. Carmack, R. Macdonald, H. Melling, J. Swift, P. Wheeler, B. Sherr, and E. Sherr (2004), The joint roles of Pacific and Atlantic-origin waters in the Canada Basin, 1997–1998, *Deep Sea Res., Part I*, *51*(1), 107–128, doi:10.1016/j.dsr.2003.09.010.

Melling, H., R. Lake, D. Topham, and D. Fissel (1984), Oceanic thermal structure in the western Canadian Arctic, *Cont. Shelf Res.*, *3*(3), 233–258, doi:10.1016/0278-4343(84)90010-4.

Padman, L., and T. M. Dillon (1987), Vertical heat fluxes through the Beaufort Sea thermohaline staircase, *J. Geophys. Res.*, *92*(C10), 10,799–10,806, doi:10.1029/JC092iC10p10799.

Padman, L., and T. M. Dillon (1988), On the horizontal extent of the Canada Basin thermohaline steps, *J. Phys. Oceanogr.*, *18*(10), 1458–1462, doi:10.1175/1520-0485(1988)018<1458:OTHEOT>2.0.CO;2.

Padman, L., and T. M. Dillon (1989), Thermal microstructure and internal waves in the Canada Basin diffusive staircase, *Deep Sea Res., Part A*, *36*(4), 531–542, doi:10.1016/0198-0149(89)90004-6.

Perovich, D., W. Meier, M. Tschudi, S. Gerland, and J. Richter-Menge (2013), [The Arctic] Sea ice cover [in State of the Climate in 2012], *Bull. Am. Meteorol. Soc.*, *94*(8), S126–S128.

Polyakov, I. V., A. V. Pnyushkov, R. Rember, V. V. Ivanov, Y.-D. Lenn, L. Padman, and E. C. Carmack (2012), Mooring-based observations of double-diffusive staircases over the Laptev Sea slope, *J. Phys. Oceanogr.*, *42*(1), 95–109, doi:10.1175/2011JPO4606.1.

Proshutinsky, A., R. Krishfield, M.-L. Timmermans, J. M. Toole, E. Carmack, F. McLaughlin, W. J. Williams, S. Zimmermann, M. Itoh, and K. Shimada (2009), Beaufort Gyre freshwater reservoir: State and variability from observations, *J. Geophys. Res.*, *114*, C00A10, doi:10.1029/2008JC005104.

Radko, T. (2007), Mechanics of merging events for a series of layers in a stratified turbulent fluid, *J. Fluid Mech.*, *577*, 251–273, doi:10.1017/S0022112007004703.

Radko, T. (2013), *Double-Diffusive Convection*, 344 pp., Cambridge Univ. Press, New York.

Rippeth, T. P., B. J. Lincoln, Y.-D. Lenn, J. M. Green, A. Sundfjord, and S. Bacon (2015), Tide-mediated warming of Arctic halocline by Atlantic heat fluxes over rough topography, *Nat. Geosci.*, *8*(3), 191–194, doi:10.1038/ngeo2350.

Rudels, B., E. Jones, L. Anderson, and G. Kattner (1994), On the intermediate depth waters of the Arctic Ocean, in *The Polar Oceans and Their Role in Shaping the Global Environment*, edited by O. Johannessen, R. Muench, and J. Overland, pp. 33–46, AGU, Washington, D. C., doi:10.1029/GM085p0033.

Rudels, B., G. Björk, R. D. Muench, and U. Schauer (1999), Double-diffusive layering in the Eurasian Basin of the Arctic Ocean, *J. Mar. Syst.*, *21*(1), 3–27, doi:10.1016/S0924-7963(99)00003-2.

Rudels, B., E. P. Jones, U. Schauer, and P. Eriksson (2004), Atlantic sources of the Arctic Ocean surface and halocline waters, *Polar Res.*, *23*(2), 181–208, doi:10.1111/j.1751-8369.2004.tb00007.x.

Schmitt, R. W. (1994), Double diffusion in oceanography, *Annu. Rev. Fluid Mech.*, *26*(1), 255–285, doi:10.1146/annurev.fl.26.010194.001351.

Sommer, T., J. R. Carpenter, M. Schmid, R. G. Lueck, M. Schurter, and A. Wüest (2013), Interface structure and flux laws in a natural double-diffusive layering, *J. Geophys. Res. Oceans*, *118*, 6092–6106, doi:10.1002/2013JC009166.

Sommer, T., J. R. Carpenter, and A. Wüest (2014), Double-diffusive interfaces in Lake Kivu reproduced by direct numerical simulations, *Geophys. Res. Lett.*, *41*, 5114–5121, doi:10.1002/2014GL060716.

Timmermans, M.-L., J. M. Toole, R. Krishfield, and P. Winsor (2008), Ice-Tethered Profiler observations of the double-diffusive staircase in the Canada Basin thermocline, *J. Geophys. Res. Oceans*, *113*, C00A02, doi:10.1029/2008JC004829.

Toole, J. M., R. A. Krishfield, M.-L. Timmermans, and A. Proshutinsky (2011), The Ice-Tethered Profiler: Argo of the Arctic, *Oceanography*, *24*(3), 126–135, doi:10.5670/oceanog.2011.64.

Turner, J. (1965), The coupled turbulent transports of salt and heat across a sharp density interface, *Int. J. Heat Mass Transfer*, *8*(5), 759–767, doi:10.1016/0017-9310(65)90022-0.

Turner, J., and H. Stommel (1964), A new case of convection in the presence of combined vertical salinity and temperature gradients, *Proc. Natl. Acad. Sci. U. S. A.*, *52*(1), 49–53, doi:10.1073/pnas.52.1.49.

Walsh, D., and E. Carmack (2003), The nested structure of Arctic thermohaline intrusions, *Ocean Modell.*, *5*(3), 267–289, doi:10.1016/S1463-5003(02)00056-2.